Master Thesis

Signal and background studies for scalar leptoquark pair production in the $t\bar{t} + 2\tau$ channel at the ATLAS experiment

Daniel Adlkofer

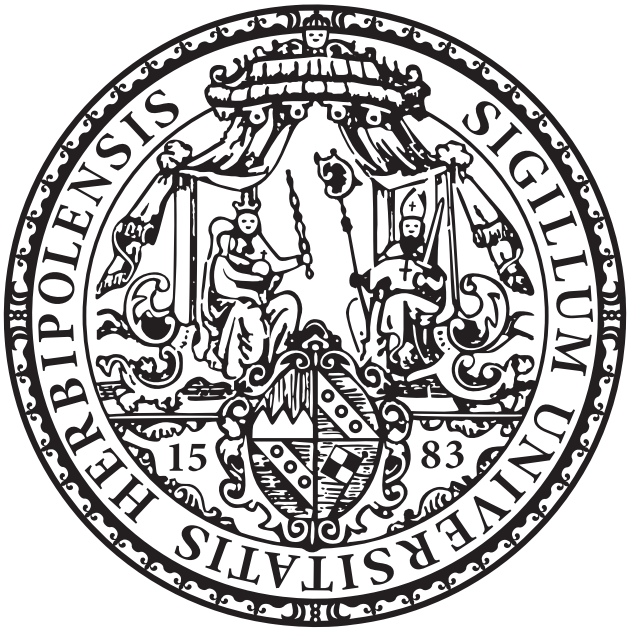

Supervisor
Prof. Dr. Raimund Ströhmer

Advisor
Dr. Mahsana Haleem

December 2018

Physikalisches Institut
Lehrstuhl für Physik und ihre Didaktik
Julius-Maximilians-Universität Würzburg

Contents

1

XyZ

sample	$\mathbf{t\bar{t}}$	$\mathbf{t\bar{t}H}$	$\mathbf{LQ}_{500\,\mathrm{GeV}}$	$\mathbf{LQ}_{1\,\mathrm{TeV}}$
selection	reconstruction	reconstruction	reconstruction	reconstruction
	event yield	event yield	event yield	event yield
≥ 2 b-jets	186 395	209	152	1.5
≥ 2 b-jets + $\geq 1\,\tau$	505	7	94	0.9
≥ 2 b-jets + $\geq 2\,\tau$	1.7	0.4	27	0.2

Table 1.1: Event yield for different selections with tau leptons for the $t\bar{t}$, the $t\bar{t}H$ and the LQ Monte Carlo sample. The luminosity account for $150\,\mathrm{fb}^{-1}$.

sample	$\mathbf{t\bar{t}}$	$\mathbf{t\bar{t}H}$
selection	efficiency $\frac{\epsilon}{\%}$	efficiency $\frac{\epsilon}{\%}$
≥ 2 b-jets	26.52	36.72
≥ 2 b-jets $+1\,\tau$	3.18	8.83
≥ 2 b-jets $+2\,\tau$	1.41	2.13

Table 1.2: Efficiencies for different selections with tau leptons for the $t\bar{t}$ and the $t\bar{t}H$ Monte Carlo sample.

sample		**$t\bar{t}$**		**$t\bar{t}H$**	
selection	reference selection	reconstruction ratio $\frac{r}{\%}$	truth ratio $\frac{r}{\%}$	reconstruction ratio $\frac{r}{\%}$	truth ratio $\frac{r}{\%}$
≥ 2 b-jets $+1\,\tau$	≥ 2 b-jets	0.28	2.35	3.43	14.26
≥ 2 b-jets $+2\,\tau$	≥ 2 b-jets	0.0011	0.020	0.24	4.11

Table 1.3: Ratios for different selections with tau leptons for the $t\bar{t}$ and the $t\bar{t}H$ Monte Carlo sample.

sample	**$t\bar{t}$**		**$t\bar{t}H$**	
selection	numerator event yield	denominator event yield	numerator event yield	denominator event yield
truth matching for tau	63	13723	5590	21610
efficiency	0.46%		25.9%	
tau from H^0, $W^{\pm}$, Z^0	0	0	4859	11988
efficiency	-		40.5%	
tau from B-mesons	63	13722	20	7416
efficiency	0.46%		0.27%	
tau within a jet	8440	3776952	18511	20327225
efficiency	0.22%		0.091%	
tau within a b-jet	6098	2658379	2317	1208924
efficiency	0.23%		0.19%	

Table 1.4: Event yield for different selections with tau leptons for the $t\bar{t}$ and the $t\bar{t}H$ Monte Carlo sample. The luminosity account for $36.1\,\text{fb}^{-1}$.

sample	**LQ**$_{500\,\mathrm{GeV}}$		**LQ**$_{1\,\mathrm{TeV}}$	
selection	numerator event yield	denominator event yield	numerator event yield	denominator event yield
truth matching for tau	2604	5362	2263	5055
efficiency	48.6%		44.8%	
tau from H^0, $W^{\pm}$, Z^0	95	340	82	461
efficiency	27.9%		17.8%	
tau from B-mesons	0	183	0	200
efficiency	0.0%		0.0%	
tau from LQ	1744	3286	1057	2022
efficiency	53.1%		52.3%	
tau within a jet	7232	55208	7011	63671
efficiency	13.1%		11.0%	
tau within a b-jet	2317	1208924	6098	2658379
efficiency	0.45%		0.23%	

Table 1.5

2

Introduction

3

Theoretical background for the search for scalar leptoquarks

This chapter describes the basic theoretical knowledge required for the search for scalar Leptoquarks including the successful Standard Model of elementary particle physics evolved from the symbiosis of experimental achievements and theoretical milestones. Besides its success some issues still remain and could be a hint to physics beyond the Standard Model, giving space to introduce the Leptoquark Model as one possible extension.

3.1 The Standard Model of particle physics

A remarkable achievement for understanding nature is the Standard Model of particle physics, embracing physics at the most fundamental level. This quantum field theory, incorporating conceptual frameworks like special relativity and quantum mechanics, describes the constituents of matter and the laws governing their interactions. [1] Despite its success of being the best theory so far capable of explaining the observed results within its domain in agreement with empirical data, it seems not to be the complete story. There are still many puzzles left which are not described by the Standard Model. That circumstance keeps physicists well motivated to gain further progress and to push the frontiers of our understanding. [2]

One of the most important concept in physics is that of symmetries, because they are deeply connected with conservation of laws, following Noether‘s Theorem. Physical properties can appear in form of an invariant under symmetry transformation, leaving that property unchanged, or as covariant, changing their property induced

by the symmetry transformation. Foundational symmetries of particle include space

group	defining property	application
$U(n)$	$n \times n$ unitary ($U^\dagger U = 1$)	$U(1)$ electromagnetism
$SU(n)$	$n \times n$ unitary ($U^\dagger U = 1$) with $\det U = 1$	$SU(2)$ weak interactions $SU(3)$ strong interactions
$SO(n)$	$n \times n$ orthogonal ($O^\intercal O = 1$) with $\det O = 1$	$SO(3)$ rotations $SO(3,1)$ Lorentz transformations

Table 3.1: Lie symmetry groups for the gauge interactions of the Standard Model [1].

translation symmetry and hence the conservation of momentum, rotational invariance and hence conservation of angular momentum as well as time translation invariance leading to energy conservation. The proper mathematical description for fundamental symmetries involves group theory. In case of particle physics almost all groups are Lie groups $\mathcal{G}$, that is a set of objects $\{g_i\}$, which can be combined with a binary operation and has four basic properties: closure, identity, inverse element and associativity. For Lie groups additionally the group elements are continuous and differentiable function of some finite set of parameter θ_a:

$$g = g(\theta_1, \ldots, \theta_N) = \exp\left[i\theta_a \mathbf{T}^a\right] = \exp\left[i\vec{\theta}\vec{\mathbf{T}}\right] \qquad \text{with} \quad a = 1, \ldots, N \tag{3.1}$$

Here $\mathbf{T}^a$ are the generators of the group from which all elements of the group can be created. The irreducible representatives of a group can be written as complex matrices*, acting on the wavefunction of the particles and on charges as well as on space-time coordinates. [1] The local symmetry $SU(3)_c \times SU(2)_L \times U(1)_Y$ summarizes the gauge interactions of the Standard Model (see table 3.1). Here c indicates the strong force, L the left handed chirality of the weak regime and $Y = B + s$ the hypercharge calculated from baryon number B and strangeness s. [3] Besides the continuous symmetries above also important discrete symmetries exist in the

*Irreducible means that not all representing matrices of the group can be decomposed into block-diagonal form simultaneously [1].

Standardmodel like parity P, referring to the transformation $\vec{x} \to -\vec{x}$, time reversal T, referring to $t \to -t$, and charge conjugation C, corresponding to the exchange of a particle with its anti-particle. The weak force breaks P and C, but not the product of CPT. [2]

Matter and its interactions can be described by two basic types of particles and the fundamental forces, i.e. the electromagnetic force, the weak and the strong force and gravity. Fermionic particles, following Fermi-Dirac statistics, make up matter, whereas bosons, following Bose-Einstein statistics, are acting as mediators of the fundamental forces. [4][5]
The fermions can be further categorized into 6 leptons l characterized through lepton quantum number L_l and 6 quarks q characterized through baryon quantum number B together with their anti-particles ($\bar{l}$ respectively $\bar{q}$). The only difference between particle and anti-particle is contrary electrical charge and contrary lepton respectively baryon number. Leptons occur in three generations with different flavour – electron (e), muon (μ) and tauon (τ) – and can carry electrical charge $Q = \pm e$ in units of the elementary charge or electrical neutral neutrinos ν_l. [5]
Table 3.2 shows the leptons with selected properties like mass. Various neutrino oscillation experiments confirm that neutrinos have non-zero masses, although the Standard Model does not predict neutrino masses [6][7]. The flavor states ν_α with $\alpha = e, \mu, \tau$ are quantum entangled with the mass states ν_i where $i = 1, 2, 3$ described by an unitary matrix $U_{\alpha i}$ [8]. Because of the absence of the right chirality spinor components, the mass term $\bar{\Psi}_L \Psi_R + \bar{\Psi}_R \Psi_L$ cannot be formed in case of neutrinos. One possible solution is to introduce very massive[†] right-chiral neutrinos, giving them the differnt masses with a Majorana mass term. This corresponds to the prediction of the seesaw meachnism. [2]
The quarks also occur in three generations and carry electrical charge $Q = \pm e$ in units of the elementary charge as well as color charge. Possible color charges are red, green and blue and the additional anti-colors indicating that quarks are interacting with the strong force among others. [5] Quarks only occur confined in color-neutral compound systems called hadrons. Baryons are three-quark states with baryon number 1 and mesons are quark-anti-quark states, having a baryon number of 0. [4] The reason for quark confinement can be found in the potential $V(r)$ between quarks and anti-quarks depending on distance r. The potential has the shape $V(r) \propto \frac{-1}{r} + \text{const} \cdot r$. When seperating a quark-anti-quark pair, additional potential energy is supplied, which can exceed at distance R the potential $V(R) > 2m_q$ for

[†]So massive that it is beyond todays oberservable mass limit [2].

leptons

l	L_l	B	Q/e	$m/\frac{\text{GeV}}{c^2}$	Spin $S_z/\hbar$
e^-	$L_e = 1$	0	-1	0.511	$\frac{1}{2}$
ν_e	$L_e = 1$	0	0	$< 2 \cdot 10^{-6}$	$\frac{1}{2}$
μ^-	$L_\mu = 1$	0	-1	106	$\frac{1}{2}$
ν_μ	$L_\mu = 1$	0	0	$< 2 \cdot 10^{-6}$	$\frac{1}{2}$
τ^-	$L_\tau = 1$	0	-1	$1.78 \cdot 10^3$	$\frac{1}{2}$
ν_τ	$L_\tau = 1$	0	0	$< 2 \cdot 10^{-6}$	$\frac{1}{2}$

quarks

q	L_l	B	Q/e	$m/\frac{\text{GeV}}{c^2}$	Spin $S_z/\hbar$
u (up)	0	$\frac{1}{3}$	$\frac{2}{3}$	2.2	$\frac{1}{2}$
d (down)	0	$\frac{1}{3}$	$-\frac{1}{3}$	4.7	$\frac{1}{2}$
c (charm)	0	$\frac{1}{3}$	$\frac{2}{3}$	$1.3 \cdot 10^3$	$\frac{1}{2}$
s (strange)	0	$\frac{1}{3}$	$-\frac{1}{3}$	95	$\frac{1}{2}$
t (top)	0	$\frac{1}{3}$	$\frac{2}{3}$	$17 \cdot 10^4$	$\frac{1}{2}$
b (bottom)	0	$\frac{1}{3}$	$-\frac{1}{3}$	$4.2 \cdot 10^3$	$\frac{1}{2}$

gauge bosons

boson	L_l	B	Q/e	$m/\frac{\text{GeV}}{c^2}$	Spin $S_z/\hbar$
γ	0	0	0	0	1
Z^0	0	0	0	91.2	1
W^-	0	0	-1	80.4	1
W^+	0	0	$+1$	80.4	1
g	0	0	0	0	1
H^0	0	0	0	125	0

Table 3.2: Overview of leptons l, quarks q and gauge bosons as mediators of the forces with some selected properties and quantum numbers like electrical charge Q, mass m, lepton number L_l and baryon number B. [2][9]. Anti-particles are not shown due to the only difference in opposite electrical charge and lepton/baryon number.

more than two quark masses. Quantum fluctuations result in the origin of a new quark pair in between, now having two pairs again externally color-neutral. [2] Table 3.2 shows the different quark flavor up, down, charm, strange, top and bottom with some characteristic properties.
The bosons shown in table 3.2 are the quanta of the fundamental forces [4]:

- The photon γ is the mediator of the electromagnetic force.
- Three mediators Z^0, W^+ and W^- for the weak force.
- 8 colored gluons as mediators for the strong force.
- The Higgs boson H^0 as quantum of the Higgs field, providing the masses for the elementary particles.

The mediator of a quantum field theory of gravity would be the graviton, altough this is hypothetically at the current state of research. A second aspect is that on elementary particle scales gravity is insignificant compared[‡] to all other forces and is therefore not originally considered in the Standard Model. [4]

Figure 3.1 summarizes the picture of the Standard Model with its fermions and bosons. The lines indicate which particles interact with each other trough the mediators, including the self-interaction.

3.2 Beyond the scope of The Standard Model

3.3 Leptoquark Models

[‡]Relative strength of gravity compared to the weak interaction accounts for 10^{-35} [1].

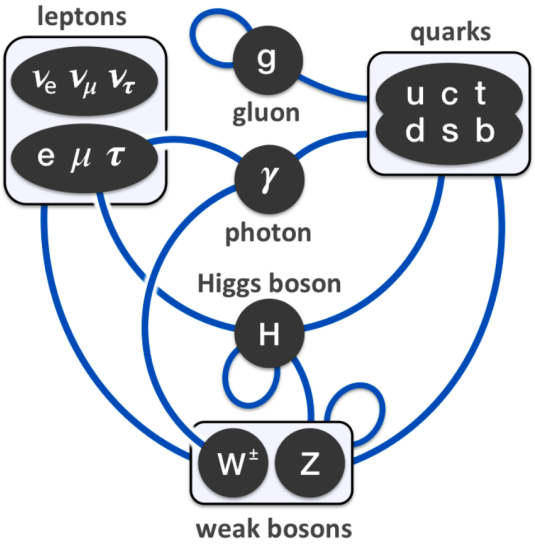

Figure 3.1: The Standard Model with its fermions and bosons and the involved interactions. The solid blue line indicates which particles interact with each other. Loops include self-interaction. [10]

4

Experimental setup for the search for scalar leptoquarks

For the search for scalar leptoquarks the ATLAS detector at the Large Hadron Collider (LHC) is used as experimental setup, which will be described within this chapter. The general setting of the proton-proton collider located at the CERN research center is the topic of section 4.1. The particle detection of the resulting collision events will take place in the ATLAS detector with its different specialized components (section 4.2). Section 4.3 addresses the leptoquark pair production in proton-proton collisions.

4.1 The Large Hadron Collider accelerator complex

The research center CERN (Conseil Européen pour la Recherche Nucléaire) was founded in 1954 near Geneva, Switzerland to become a major European joint venture on elementary particle physics. Currently 22 member states are participating in that large-scale project with the ambition to probe the essential constituents of nature and the fundamental forces acting between them. [11]

In the accelerator complex protons reach energies of 6.5 TeV by going through different accelerator stages and are brought to collisions at defined interaction sites in time intervals of 25 ns. Particle detectors then register signatures of the resulting collision events and the analysis of newly created particles gives insight to the nature of elementary particle physics.
Figure 4.1 shows the different acceleration stages. Starting from the injection, protons will gain a kinetic energy of 50 MeV in the linear accelerator LINAC2 and will be

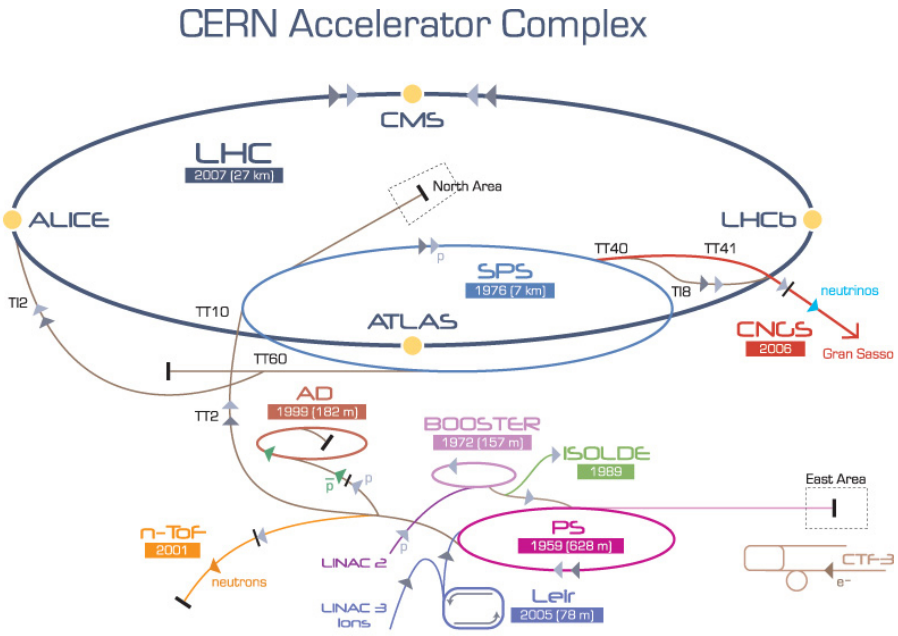

Figure 4.1: Schematic of the CERN accelerator complex with its different stages and few experiments like ATLAS located at one crossing point for protons. [12]

further transferred to the Proton Synchrotron Booster (1.4 GeV), the Proton Synchrotron (25 GeV), the Super Proton Synchrotron (450 GeV) and finally to the LHC ring with its 26.7 km circumference. [11]
The LHC is designed as two-ring proton-proton collider. Conditions for a stable proton beam are diverse, including high vacua of 10^{-10} mbar to 10^{-11} mbar and temperatures of 1.9 K for the superconducting NbTi-magnets of the accelerator. [13]

Different experiments like ALICE[14], LHCb[15] are located at the LHC due to the variety of research questions. But the subject of interest in this work lies in the high luminosity experiment ATLAS, which is specialized for proton-proton collisions, like its counterpart CMS[16]. Main tasks of ATLAS are more precise measurements of the SM (see chapter 3.1), better understanding Quantum Chromo Dynamics (QCD) and search for supersymmetric models, and new physics, among others. With the LHC production of 10^9 inelastic events per second, up to 23 simultaneously events at dominating high QCD cross sections reqiure a powerful detector that is capable of recognizing the characteristic signatures. These circumstances make up the demands for ATLAS, including fast electronic elements, high detector granularity, handling high particles fluxes and reducing overlapping events at a large acceptance and coverage region. [17]

4.2 The ATLAS detector at the LHC

One of the general purpose detector for proton-proton collisions is the ATLAS detector. This 25 m tall detector is located at one interaction point of the LHC where bunches, consisting of approximately 10^{11} protons, collide at a rate of 40 MHz [17]. The number of particles encountered per time is given by [18]

$$\dot{N} = \mathcal{L}\sigma \tag{4.1}$$

with the cross section σ for the present event and the instantantaneous luminosity $\mathcal{L}$. Given a measure for the number of collisions per unit time the instantaneous luminosity can be introduced and is often used as key parameter in collider physics [13].

$$\mathcal{L} = \frac{N_b n_b f_{\mathrm{rev}} \gamma_r}{4\pi\epsilon_n \beta^*} F \tag{4.2}$$

Where N_b is the number of particles per bunch, n_b the number of bunches per beam, f_{rev} the rotational frequency, γ_r the Lorentz factor, ϵ_n the normalized transverse beam emittance, β^* the betatron function at the collision point and F respects the geometric luminosity reduction factor due to the crossing angle at the collision point. The luminosity of ATLAS exceeded the design luminosity of $\mathcal{L} = 2.05 \times 10^{34}\,\text{cm}^{-2}\,\text{s}^{-1}$ by a factor of 2.05 on the 2$^{\text{nd}}$ of November 2017, emphasizing the great success over the years [19].

The aspiration to be sensitive to the great variety of particles governed by the fundamental forces (see chapter 3.1) influenced the detector design accordingly. The layered structure reflects the fact that The basic structure of ATLAS is shown in figure 4.2 with its different sub-detector systems together with the convention for the used coordinate system. The nominal interaction point acts as origin of the coordinate system, where the z-axis follows the beam line counterclockwise. Perpendicular to the z axis lies the transverse x-y-plane usually described through the azimuthal angle ϕ. The positive x-axis points towards the center of the LHC. The cylindric symmetry of the detector suggests a cylindric coordinate system with the angle θ starting from the beamline. [17] Since the polar angle is not a Lorentz invariant quantity, it is useful to describe the position in terms of rapidity [13] $w = \frac{1}{2} \ln \frac{E+p_z c}{E-p_z c}$ in that highly relativistic regime. In the limit of large momenta, i.e. $|\mathbf{p}|c \approx E$, the rapidity coincides with the pseudorapidity formulated as [20]

$$\eta = -\ln \tan \frac{\theta}{2}. \tag{4.3}$$

This variable has only the polar angle as dependence and is therefore the adequate quantity in the context of collision experiments, where usually the angle θ from the beamline is measured. [20]

The magnet configuration includes a superconducting solenoid with a field strength of 2 T sourrounding the inner detector as well as three large superconducting toroid magnets composed in an eight-fold azimuthal symmetry around the calorimeter. The barrel toroid magnet delivers a field strength of 0.5 T and in the end-cap a field of 1 T is present. [17]
The inner detector is responsible for pattern recognition, momentum and vertex measurements and electrically charged particle identification which is achieved with a combination of semiconductor pixel and microstrip trackers (SCT). The Insertable B-Layer (IBL) is the innermost layer of the pixel detectors at a radius of 3.3 cm away from the beam line. Additional straw tube tracking detectors are sensitive to tran-

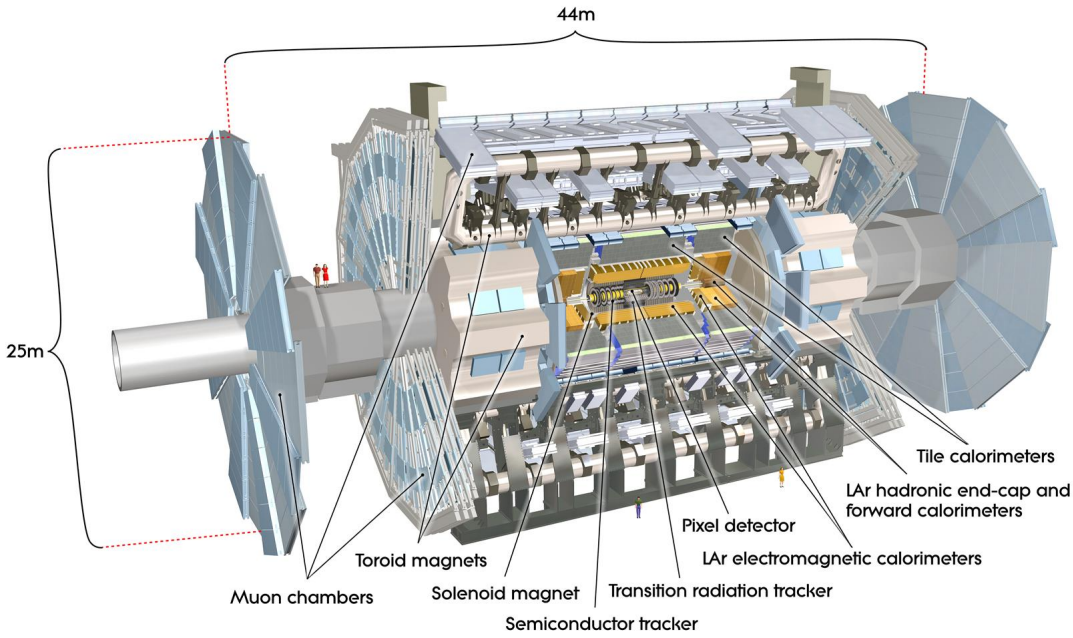

(a) The layered structure of the ATLAS Detector at the LHC with its sub-systems Inner Detector, Calorimeter, magnets and Muon Spectrometer [17].

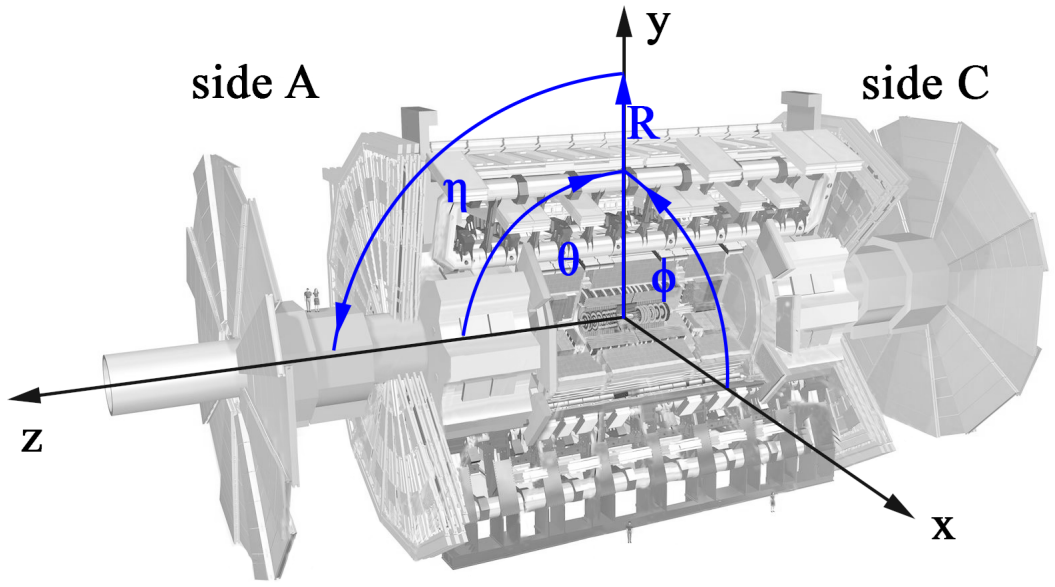

(b) The global ATLAS coordinate system formulated in cylindric coordinates with the z-axis parallel to the beam line and the transverse plane defined through azimuthal angle ϕ and pseudorapidity η. Based on [17].

Figure 4.2: Structure of the ATLAS detector and the used coordinate system.

sistion radiation (TRT) in the outer part that are responsible for high vertex and momentum resolution. The $R-\phi$ segmented pixel detectors are of size $50 \times 400\,\mu m^2$ and the SCTs with its 8 strip layers cover together a range of $|\eta| < 2.5$. Typically 36 hits per track are provided by the 4 mm straw tubes of the TRTs, which cover the range $|\eta| \leq 2.0$. [21][17]
Liquid argon electromagnetic sampling **calorimeters** with high granularity allow an excellent energy measurement for electrons and photons. It has a total thickness of more than 22 radiation lengths X_0 in the barrel region ($|\eta| < 1.475$) and more than $24X_0$ in the end-cap region ($1.375 < |\eta| < 3.2$). For hadronic energy measurements a scintillator-tile calorimeter covering $|\eta| < 1.7$ is in operation. It is a sampling calorimeter and uses steel as absorber material and scintillating tiles as active material in conjunction with wavelength shifting fibres. Further LAr technology is used for hadronic particles in the outer pseudorapidity range up to $|\eta| = 3.2$. Here copper plates provide the absorber material. The forward calorimeters extend the coverage for hadronic and electromagnetic energy measurements to $|\eta| = 4.9$ and are $10X_0$ deep. [17]
The **muon system** is suited in the outer layer of ATLAS and provides as independent system resolution for high energy muon tracks with three layered precision chambers. This is possible because of the air-cored toroid magnet system including one barrel and two end-cap magnets generating strong bending power in a large volume and delivering a mostly perpendicular magnetic field regarding the muon trajectories. The bending power $\int \vec{B} d\vec{l}$ along the track of the muon $d\vec{l}$ reaches 1.5 T m to 5.5 T m in the range $|\eta| < 1.4$ (barrel) and up to 7.5 T m (end-cap). The precision chambers are Monitored Drift Tubes (MDT) and in the larger pseudorapidity range Chathode Strip Chambers (CSC) which are multiwire proportional chambers. Due to the fact that the overall performance depends crucially on the alignment of the muon detectors with respect to each other and in respect to the Inner Detector, MDTs are equipped with a optical monitoring system with 1200 sensors. Resistive Plate Chambers (RPC) and Thin Gap Chambers (TGC) are the constituents of the muon trigger system. [17]
Due to technology and resource limitations the data recording rate has to be reduced from 40 MHz to 200 Hz. This poses high demands on an efficient **trigger system** which is organised in three levels. Level 1 uses only a subset of the total detector information making basic decisions to flag so called regions of interest, i.e. coordinate regions. Searches include patterns for high transverse momenta of muon tracks, electrons and photons as well as jets or large missing energy balances. The output rate after this first selection accounts for 75 kHz. The high level trigger 2 and 3 are responsible for selecting the level 1 triggerd regions at full granularity and

precision. The level 3 event filter is the final stage and achieves data reduction down to the final data-taking rate of 200 Hz, writing events of the size of approximately 1.3 MB to the disks. The event filter's selection criteria are implemented using offline analysis procedures. [17]

4.3 Leptoquark pair production in proton-proton collisions

5

Turning detector signatures into physical objects

5.1 b-tagging at ALTAS – identifying b-jets

The third generation quarks, i.e. top (t) and bottom (b), play a crucial role in the Standard Model and its various extension possibilities like the Leptoquark Model due to their large masses [22]. Therefore, it is essential to identify hadrons containing b quarks and seperating them from light-flavour quarks at hadron collider detectors like ATLAS. This task is commonly reffered as b-tagging and can be seen as a classification problem with the goal to assign right jet flavours. To that end the particle tracks in the Inner Detector and the jet reconstruction of clusters in the electromagnetic and hadronic calorimeter are discriminating objects. [23]

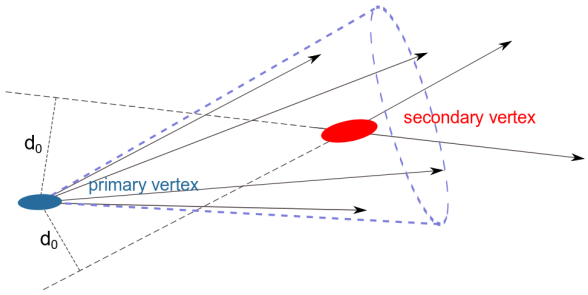

Figure 5.1: Signature of a b-jet with the primary and secondary vertex created relevant for b-tagging. d_0 is the impact parameter. [22]

The long lifetime of B hadrons in the order of 1.6 ps allow them to travel a few millimeters in the detector. The subsequent decay of those heavy particles within

a secondary vertex produce tracks with comparably large impact parameter d_0 that is the shortest distance of the particle track from the primary vertex (see figure 5.1). This signature and the deduced impact parameter significance $S(d_0) = \frac{d_o}{\sigma(d_0)}$, where $\sigma(d_0)$ is the uncertainty of the impact parameter, are used by the b-tagging algorithms including five low-level and two high-level taggers. [22] The b-tagging algorithms rely on multivariate combinations of the information and process them to calculate a discriminant value for each jet. Thresholds on these values are then defining the working point to provide efficiencient identification of b-jets. For better information processing of the combinations of large input parameters neural network classes are used. [24] One example for such a trained network is the MV2 tagger which uses 24 input variables of the low-level taggers together with kinematic properties*. [23]

*For further details on MV2 see [25]

6

Data analysis

6.1 Current status in the search for scalar leptoquarks

6.2 Starting point and research question for the analysis

6.3 Used data and Monte Carlo samples

6.4 Physical object selection

6.5 Event selection

7

Results

8

Outlook

List of Figures

List of Tables

Bibliography

[1] Robert Mann. *An Introduction to Particle Physics and the Standard Model* -. CRC Press, Boca Raton, Fla, 2011.

[2] V Parameswaran Nair. *Concepts in Particle Physics - A Concise Introduction to the Standard Model*. World Scientific Publishing Company, Singapore, 2017.

[3] Ian Brock and Thomas Schörner-Sadenius. *Physics at the Terascale*. Wiley, New York, 2011.

[4] W. N. Cottingham and D. A. Greenwood. *An Introduction to the Standard Model of Particle Physics* -. Cambridge University Press, Cambridge, 2007.

[5] David Griffiths. *Introduction to Elementary Particles* -. Wiley, New York, 2. aufl. edition, 2008.

[6] Y. Fukuda et al. Evidence for oscillation of atmospheric neutrinos. *Phys. Rev. Lett.*, 81:1562–1567, Aug 1998.

[7] Q. R. Ahmad et al. Direct evidence for neutrino flavor transformation from neutral-current interactions in the sudbury neutrino observatory. *Phys. Rev. Lett.*, 89:011301, Jun 2002.

[8] G. L. Fogli, E. Lisi, A. Marrone, D. Montanino, A. Palazzo, and A. M. Rotunno. Global analysis of neutrino masses, mixings and phases: entering the era of leptonic CP violation searches. *Phys. Rev.*, D86:013012, 2012.

[9] M. Tanabashi et al. Review of particle physics. *Phys. Rev. D*, 98:030001, Aug 2018.

[10] Maksym Teklishyn. Measurement of the η c (1s) production cross-section via the decay η c to proton-antiproton final state. 09 2014.

[11] CERN. About CERN. `https://home.cern/about`. retrieved on September 4, 2018.

[12] CERN. CERN Complex. `http://www.lhc-facts.ch/img/news2015/lhccomplex_.jpg`. Last update: October 29, 2011.

[13] Lyndon Evans and Philip Bryant. LHC Machine. *Journal of Instrumentation*, 3(08):S08001, 2008.

[14] The ALICE Collaboration, K Aamodt, et al. The ALICE experiment at the CERN LHC. *Journal of Instrumentation*, 3(08):S08002, 2008.

[15] The LHCb Collaboration, A Augusto Alves Jr, et al. The LHCb Detector at the LHC. *Journal of Instrumentation*, 3(08):S08005, 2008.

[16] The CMS Collaboration, S Chatrchyan, et al. The CMS experiment at the CERN LHC. *Journal of Instrumentation*, 3(08):S08004, 2008.

[17] The ATLAS Collaboration, G Aad, et al. The ATLAS Experiment at the CERN Large Hadron Collider. *Journal of Instrumentation*, 3(08):S08003, 2008.

[18] Donald H. Perkins. *Introduction to High Energy Physics* -. Cambridge University Press, Cambridge, 4^{th} edition, 2000.

[19] Rende Steerenberg. LHC report: LHC reaches 2017 targets. `https://home.cern/cern-people/updates/2017/11/lhc-report-lhc-reaches-2017-targets`. posted by Stefania Pandolfi on 7 Nov 2017. Last updated 26 Jun 2018.

[20] Cheuk-Yin Wong. *Introduction to High-Energy Heavy-Ion Collisions*. WORLD SCIENTIFIC, 1994.

[21] Alessandro La Rosa. The ATLAS Insertable B-Layer: from construction to operation. *JINST*, 11(12):C12036, 2016.

[22] Per Ola Hansson Adrian. The ATLAS b-Jet Trigger. In *Proceedings, 31st International Conference on Physics in collisions (PIC 2011): Vancouver, Canada, August 28-September 1, 2011*, 2011.

[23] Michela Paganini. Machine Learning Algorithms for b-Jet Tagging at the ATLAS Experiment. In *18th International Workshop on Advanced Computing and Analysis Techniques in Physics Research (ACAT 2017) Seattle, WA, USA, August 21-25, 2017*, 2017.

[24] Luca Scodellaro. b tagging in ATLAS and CMS. In *5th Large Hadron Collider Physics Conference (LHCP 2017) Shanghai, China, May 15-20, 2017*, 2017.

[25] Expected performance of the ATLAS b-tagging algorithms in Run-2. Technical Report ATL-PHYS-PUB-2015-022, CERN, Geneva, Jul 2015.